

Stem-root flow effect on soil-atmosphere interactions and uncertainty assessments

Tzu-Hsien Kuo¹, Jen-Ping Chen¹, and Yongkang Xue²

¹ Department of Atmospheric Sciences, National Taiwan University, Taipei, Taiwan, R.O.C.

² Department of Atmospheric and Oceanic Sciences, and Department of Geography,
University of California, Los Angeles, California, U.S.A.

* Corresponding Author:

Jen-Ping Chen, Professor

Department of Atmospheric Sciences, National Taiwan University

No. 1, Sect. 4, Roosevelt Road, Taipei, Taiwan 10673

Email: jpchen@as.ntu.edu.tw

Phone: +886-2-33663912; Fax: +886-2-23633317

Abstract

Rainfall that reaches the soil surface can rapidly move into deeper layers via vertical redistribution of soil moisture through the stem-root flow mechanism. This study develops the stem-root flow parameterization scheme and coupled this scheme with the Simplified Simple Biosphere model (SSiB) to analyze its effects on land-atmospheric interactions. The SSiB model was tested in a single column mode using the Lien Hua Chih (LHC) measurements conducted in Taiwan and HAPEX-Mobilhy (HAPEX) measurements in France. The results show that stem-root flow generally caused a decrease in soil moisture at the top soil layer and moistened the deeper soil layers. Such soil moisture redistribution results in substantial changes in heat flux exchange between land and atmosphere. In the humid environment at LHC, the stem-root flow effect on transpiration was minimal, and the main influence on energy flux was through reduced soil evaporation that led to higher soil temperature and greater sensible heat flux. In the Mediterranean environment of HAPEX, the stem-root flow substantially affected plant transpiration and soil evaporation, as well as associated changes in canopy and soil temperatures. However, the effect on transpiration could be either positive or negative depending on the relative changes in the soil moisture of the top soil versus deeper soil layers due to stem-root flow and soil moisture diffusion processes.

Key words: stemflow, root flow, soil moisture, evapotranspiration, land-atmospheric interaction, SSiB

20 1. Introduction

21 The water stored in the land system is a key factor controlling many physical processes and
22 feedback between the land and atmosphere. Soil moisture is a source of water for the atmosphere
23 through processes that lead to evapotranspiration, including bare soil evaporation, plant transpiration
24 and evaporation from other surfaces such as leaves, snow, etc. The rainfall redistribution process in
25 forest systems affects soil moisture amount and its distribution (McGuffie et al., 1995; Chase et al.,
26 1996; Chase et al., 2000; Zhao et al., 2001). Rain water entering the forest is redistributed via
27 several pathways before reaching the forest floor, e.g., some is intercepted by the canopy and some
28 reaches the soil as throughfall. A significant amount of rainwater intercepted by the canopy can flow
29 down along tree stems and reach the forest floor in a process termed stemflow. The efficiency of
30 stemflow varies with plant species, seasons, meteorological conditions, rainfall intensity, and canopy
31 structure (Levia and Frost, 2003; Levia and Germer, 2015). Johnson and Lehmann (2006)
32 summarized various field measurements and showed that the fraction of precipitation that becomes
33 stemflow ranges from 0.07% to 22%.

34 In contrast to the throughfall that infiltrates slowly through the top soil, stemflow can continue via
35 the root system (hereafter called the “stem-root flow”) and quickly reach deep soil layers and the water
36 table (Liang et al., 2007; 2009). It has long been recognized that the stem-root flow can help to store
37 water in deeper soil layers and thus create favorable conditions for plant growth under arid conditions
38 (Návar, 1993; Li et al., 2009). Soil moisture redistribution by stem-root flow not only affects

39 vegetation growth but also land evapotranspiration and runoff (Neave and Abrahams, 2002).
40 Furthermore, the enhanced water penetration can significantly alter groundwater recharge. Taniguchi
41 et al. (1996) showed that in a pine forest, the stem-root flow contributed approximately 10–20% of
42 annual groundwater recharge even with a stemflow-to-precipitation ratio of only 1%.

43 Stem-root flow effects have not been considered in most land-surface schemes of climate models.
44 Tanaka et al. (1996) developed a model to evaluate the effect of stem-root flow on groundwater. This
45 model is yet to be implemented in current land surface models. Li et al. (2012) pointed out that
46 stemflow hydrology and preferential flow along roots are intimately linked, but direct integration of
47 these processes into land models, to our knowledge, has not been reported.

48 In this paper, we parameterized the stem-root flow processes in a land surface model named the
49 Simplified Simple Biosphere Model (SSiB; Xue et al., 1991), and analyzed how stem-root flow affects
50 soil moisture and whether this effect is significant enough to influence atmospheric processes. Soil
51 moisture data from two sites, located at Lien Hua Chih, Taiwan (LHC) and Bordeaux/Toulouse, France
52 (from the HAPEX-Mobilhy experiment, hereafter called HAPEX), were collected for model
53 evaluation. The two sites represent different climate regimes and terrestrial ecosystem, and stem-root
54 flow modifies their surface energy and water processes in somewhat dissimilar ways.

55

56 2. Methodology

57 2.1 The stem-root flow model

58 In the original SSiB land surface model (Xue et al., 1996), vertical soil moisture movement is
 59 described by the diffusion equations:

$$\begin{aligned}
 \frac{\partial \theta_1}{\partial t} &= \frac{1}{D_1} [P + Q_{12} - E_{SE} - b_1 E_{TR,1}] \\
 \frac{\partial \theta_2}{\partial t} &= \frac{1}{D_2} [-Q_{12} + Q_{23} - b_2 E_{TR,2}] \\
 \frac{\partial \theta_3}{\partial t} &= \frac{1}{D_3} [-Q_{23} + Q_3 - b_3 E_{TR,3}]
 \end{aligned} \tag{1}$$

61 where the subscripts 1, 2 and 3 are indices of the top, middle, and bottom soil layers, respectively; θ is
 62 the soil moisture content, expressed as a fraction of the saturated value; D is soil thickness; P is
 63 effective precipitation flux on the soil surface, composed of the direct throughfall and the throughfall
 64 from leave-intercepted rainfall (cf. Fig. 1); $Q_{ij} = -k[\partial\Psi/\partial z + 1]$ is the flux of water between the i^{th}
 65 and j^{th} layers, and is defined to be positive in an upward direction; Ψ (in m) is the soil water potential;
 66 E_{SE} is the evaporation rate of bare soil; i is the soil layer index; $E_{TR,i}$ is the transpiration rate in soil
 67 layer; b_i is the proportionality factor that accounts for root distribution; Q_3 is the water flux entering the
 68 water table. The similar approach has been used by many land surface models. Note that the middle
 69 soil layer can be divided into more sublayers with similar formula as used for the middle layer. In
 70 these equations, the transfer velocity Q_{ij} considers only the soil diffusion flow. This study develops
 71 the parameterizations that include the stem-root flow mechanism which provides a “bypass” for water
 72 to channel through the soil on root surfaces (Fig. 1). The stemflow reaching the top soil layer, q_0 , is
 73 often represented as a fraction of the total precipitation (or, more precisely, the leaf drainage) such that
 74 direct rainfall entering the soil becomes

$$P' \equiv P - q_0. \tag{2}$$

76 By relating the stemflow to leaf drainage, there is an implicit threshold for stemflow initiation that
 77 corresponding to the threshold of leaf drainage.

78 After entering the soil, the root flow is divided into a downward transfer flux q_z (within the root
 79 system) and a lateral transfer flux q_x (from the root surface to the soil). These two fluxes can be
 80 parameterized as following:

$$81 \quad q_{z,i} = \alpha_z A_i h_i V_s \quad (3)$$

$$82 \quad q_{x,i} = \begin{cases} \alpha_x R_i A_i K(\Psi_i) \left(\frac{\Psi_i - \Psi_s}{D_{\text{eff}}} \right), & \text{if } h_i > 0 \\ 0, & \text{if } h_i = 0 \end{cases} \quad (4)$$

83 where α_z and α_x are proportionality coefficients; A_i (in $\text{m}^2 \text{m}^{-3}$) is the total root surface area density that
 84 varies with vegetation types (Böhm, 1979; Zhang et al., 2005; Li et al., 2013); h_i (in m) is the thickness
 85 of water on the root surface; V_s (in m s^{-1}) is the terminal velocity of root flow; R_i (in m) is the root
 86 length; K (in m s^{-1}) is the hydraulic conductivity of the soil; Ψ_s (in m) is the soil water potential at
 87 saturation; Ψ_i (in m) is the soil water potential; and D_{eff} (in m) is the effective thickness of the
 88 water-soil interface. Derivation of D_{eff} is described in the appendix. Due to a lack of observational
 89 data, we used a vertically uniform root distribution. However, different root depths were used based
 90 on the measurements (100 cm for LHC and 140 cm for HAPEX). Note that $q_0 = q_{x,1} + q_{z,1}$
 91 according to the mass conservation principle. From Eqs. (1), (2), and (4), we have:

$$92 \quad \begin{aligned} \frac{\partial \theta_1}{\partial t} &= \frac{1}{D_1} [P' + Q_{12} - E_{SE} - b_1 E_{TR,1} + q_{x,1}] \\ \frac{\partial \theta_2}{\partial t} &= \frac{1}{D_2} [-Q_{12} + Q_{23} - b_2 E_{TR,2} + q_{x,2}] \\ \frac{\partial \theta_3}{\partial t} &= \frac{1}{D_3} [-Q_{23} + Q_3 - b_3 E_{TR,3} + q_{x,3}] \end{aligned} \quad (5)$$

93 The changes in root surface water thickness h_i obey the mass conservation principle and thus are
 94 controlled by the vertical and horizontal fluxes of root flow. Its tendency can be described as:

$$95 \quad \frac{dh_i}{dt} = \begin{cases} \frac{(q_{z,i-1} - q_{z,i} - q_{x,i})}{A_i R_i}, & \text{if } h_i > 0 \\ 0, & \text{if } h_i = 0 \end{cases} \quad (6)$$

96 Equations (5) and (6) represent the water budgets in the soil and root flow systems, respectively, and
 97 they are linked through the term q_x in Eq. (4).

98 Stemflow input into the first soil layer (q_0) is represented as a fraction of the leaf drainage (LD),
 99 which is the portion of precipitation that is intercepted by the canopy minus leaf evaporation and can
 100 be calculated in SSiB. LD is similar to canopy drip in some other models, and is represented mainly
 101 as a function of the leaf area index (LAI). The ratio of q_0 to LD depends mainly on plant type, as well
 102 as meteorological conditions such as wind speed (Levia and Frost, 2003; Johnson and Lehmann, 2006;
 103 André et al., 2008; Siegert and Levia, 2014). Unfortunately, there is still insufficient information to
 104 determine the ratio of q_0 and LD. We conducted a series of sensitivity tests with systematically
 105 varying ratio between the q_0 to LD to assess the uncertainty.

106 The stem-root flow parameterization was tested using the offline SSiB, which is a simplified
 107 version of the land-biosphere model developed by Sellers et al. (1986). The model recognizes 12
 108 different vegetation types according to Dorman and Sellers (1989), and is set up with 3 soil layers and
 109 1 canopy layer. The SSiB model has 8 prognostic variables: soil wetness for 3 layers; temperature at
 110 the canopy, ground surface and deep soil layers; snow depth at ground level; and water intercepted by
 111 the canopy. An additional variable – h_i – was added for each soil layer to account for the stem-root

112 flow mechanism. An implicit backward scheme was used to calculate the temperature tendency in the
113 coupling of the lowest atmospheric model layer with SSiB, such that energy conservation between the
114 land surface and the atmosphere was satisfied. Soil temperature was calculated using the
115 force-restore method, and water movement in the soil was described by the diffusion equation as
116 shown in Eq. (5).

117 Following typical offline simulation procedures for single-column land surface model, in situ
118 atmospheric data were applied to drive the SSiB model in 30 min time resolution. These specified
119 variables include pressure, temperature, humidity, wind speed, net radiation and rainfall. Soil
120 conditions were initialized with each site's measurement data. Fully coupled land surface model
121 typically require a couple of months to over a year to spin up the model, but the spin up time can be
122 shorter when running in off-line (single column) mode and with good initial soil conditions (de
123 Goncalves et al., 2006; Yang et al., 2011; Lim et al., 2012; Angevine et al., 2014). Our simulations
124 applied measurement data for model initialization, and the results show that the soil conditions
125 reached physical balance within a few weeks. So, at the last 10 months results of our simulations
126 are reliable.

127 2.2 Experimental design and site information

128 Two sites with different climate and vegetation conditions were selected to test the stem-root flow
129 parameterizations in the SSiB model. The first is a site with warm-to-temperate mountain rainforest
130 condition from the Lien Hua Chi (LHC; 23°55'N, 120°53'E), Taiwan. LHC is located in the Central

131 Mountain Range of Taiwan, with a hilly terrain and a mean altitude of 770 m above sea level in the
132 surroundings. The average annual rainfall at LHC is 2317 mm, with rain falling predominantly in late
133 summer and early autumn (Fig. 2). With ample rainfall, LHC is covered with dense forest with an
134 average canopy height of approximately 17 m. The vegetation cover is comprised of mixed
135 evergreens and hardwood species, including *Cryptocarya chinensis*, *Engelhardtia roxburghiana*,
136 *Tutcheria shinkoensis*, and *Helicia formosana*. The soil has a loamy texture with an average bulk
137 density of 1.29 g cm^{-3} and a porosity of 0.53 over the top 1.0 m (Chen, 2012). Soil moisture
138 measurements were collected at depths of 10, 30, 50, 70 and 90 cm.

139 The second is the HAPEX-Mobilhy data collected at the Caumont site (SAMER station No. 3;
140 $43^{\circ}41'N$, $0^{\circ}6'W$) with an elevation of 113 m above sea level and relatively flat terrain. This site has a
141 Mediterranean climate, with an annual rainfall of 856 mm, most of which occurs in spring and winter
142 (Fig. 3). In contrast to the LHC site with dense forest, the HAPEX site is covered mostly with short
143 and sparse soya crops, and the surface albedo stays nearly constant at 0.20 throughout the year
144 (Goutorbe et al., 1989). The soil type is mainly silt, mixed with sand and clay (see Table 1). Soil
145 moisture content was measured every 10 cm from the surface to a depth of 1.6 m using neutron
146 sounding probes on a weekly basis (Goutorbe, 1991; Goutorbe and Tarrieu, 1991). Note that the
147 HAPEX data have higher vertical resolution in the soil column but lower temporal resolution
148 compared with the LHC data. To simplify comparisons, the soil moisture data were converted into
149 three vertical layers. For the HAPEX data, the top (SM1), middle (SM2) and bottom (SM3) layers

150 correspond to the 0–20 cm, 20–50 cm, and 50–150 cm depths, respectively. For LHC, SM1
151 corresponds to a depth of 10 cm, SM2 is the average of the 30 cm and 50 cm soil layers, and SM3
152 corresponds to a depth of 90 cm.

153 Figures 2 and 3 show the seasonal variations of precipitation and soil moisture at different depths.
154 It is generally expected that soil moisture response to rainfall should be faster in the upper than in the
155 lower layers. However, the LHC measurements (Fig. 2) showed that the soil moisture fluctuation was
156 stronger in the middle layer than in the upper layer during the dry season when the soil moisture was
157 not saturated. Fluctuations were not obvious in rainy seasons when SM2 and SM3 are almost
158 saturated. This phenomenon is likely an indication of the preferential flow due to the root flow
159 mechanism. This phenomena, however, was not observed in the HAPEX data (Fig. 3), which may be
160 due to the coarse temporal resolution (weekly) of the data or a weaker root flow effect from the soya
161 crop, and the latter will be discussed later.

162 To test the response of soil moisture to precipitation in these two sites using the modified SSiB
163 model, a set of parameters have to be selected. These include the soil and terrain properties listed in
164 Table 1, as well as the monthly LAI coefficients in Table 2. In addition, some parameters in Eqs.
165 (3)-(6) have to be decided. Two required but little-known parameters are the root-flow velocity V_s
166 and the stemflow to leaf drainage ratio (SLR; i.e., q_0/LD). The root-flow velocity V_s is related to root
167 structure and soil texture, but such information is very limited. Studies have indicated that water flow
168 in the root-channel is approximately 100 times higher than the soil diffusion flow (Beven and Germann,

169 1982; Liu et al., 1994; Jarvis and Dubus, 2006; Köhne et al., 2009; Gerke, 2014). The maximum soil
170 diffusion flow can be represented by the saturated hydraulic conductivity, which was measured as
171 $4 \times 10^{-6} \text{ m s}^{-1}$ at HAPEX and $1 \times 10^{-6} \text{ m s}^{-1}$ at LHC. Therefore, we set the root-flow velocity V_s as
172 10^{-4} m s^{-1} in the simulation, and will discuss the associated uncertainty later.

173 The SLR value depends on a number of parameters as discussed in the previous section. This
174 study evaluated SLR-introduced uncertainty by conducting sensitivity tests with systematically
175 varying SLR from 0 to 100%, and identified optimal value that yielded the best soil moisture profiles
176 compared with the observations. The optimal SLR value for the HAPEX experiment was
177 approximately 50%, compared with 90% for the LHC case. These values reflect the large contrast in
178 leaf coverage and plant type between the two sites. In these experiments, we set A_i to $0.5 \text{ m}^2 \text{ m}^{-3}$
179 based on the Li et al. (2013) and the proportionality coefficients, α_z and α_x , are set to 1. The
180 uncertainty discussion for V_s and SLR should include the uncertainty caused by these parameters.
181 When more observational data are available, we could revisit these issues further. All simulations
182 used integration time step of 30 minutes.

183

184 3. Effect of stem-root flow on soil moisture

185 The modified SSiB model was used to simulate the intra-annual variations in soil conditions for
186 the 2010 LHC case and the 1986 HAPEX case. For the LHC case, the simulation well captured the
187 soil moisture increase associated with precipitation events followed by rapid drying (Fig. 4). Changes

188 in SM1, SM2 and SM3 all reached the 95% confidence level in all seasons. In many instances, the
189 simulated soil moisture fluctuation was stronger in the middle layer than in the top or bottom layers, as
190 found in the observations. The shading shows the range of values enclosed by the two extremes of
191 SLR (i.e., 0% and 100%). Results with other SLR ratios (not shown) generally lie within these limits
192 but may occasionally fall out of bound, indicating some nonlinearities. When SLR is zero, which has
193 no stem flow effect and is referred to as the control run in this paper, the soil moisture of the middle
194 layer is very low and fluctuates less in response to rainfall events (Fig. 4). The simulation generally
195 underestimated the soil moisture in the bottom layer even with the root-flow mechanism. In the top
196 layer, the model overestimated soil moisture in spring and winter, but underestimated it during autumn.
197 Such discrepancies are generally less substantial when the stem-root flow mechanism is included, as
198 indicated by the generally lower bias and root-mean-square error shown in Table 3. The possible
199 causes of error will be elaborated in the discussion section.

200 For the HAPEX case, the simulations also well captured the seasonal cycle as well as the sharp
201 fluctuations in the top layer (Fig. 5). The responses of SM2 and SM3 to the stem-root flow are
202 statistically significant (>95% confidence) during late summer and autumn (the main growing season
203 and relatively dry soil); whereas the responses in SM1 reached only 94% confidence level. Without
204 the stem-root flow mechanism, soil moisture was generally overestimated in the two upper layers and
205 underestimated in the bottom layer, except during April and May when all layers were too dry. When
206 stem-root flow with SLR=50% was considered, the model performed better in all layers (see Table 3).

207 Stem-root flow with a much higher SLR (e.g., SLR=100%) produced worse results for soil moisture in
208 the surface and middle layers. Note that SLR=50% produced the driest middle layer, indicating that
209 the stem-root flow effect is nonlinear because both stem-root flow and diffusion, as well as their
210 interactions, play role in soil moisture variations. Note that SSiB does not consider the potential role
211 of plant uptake, which might be potentially important in the middle layer. In the bottom layer, more
212 accurate soil moisture was obtained with SLR=100%, but this does not necessarily mean that the
213 stem-root flow was underestimated. The overestimation of soil moisture in SM1 and the
214 underestimation in SM3 in spring may be coupled, due to mechanisms that are missing in our model.
215 This issue will be elaborated in the discussion section.

216 It is also worth mentioning that both the observation and simulation showed weaker soil moisture
217 fluctuations in the middle than in the surface layer, a feature very different from the LHC case. It is
218 likely that there is a weaker stem-root flow associated with plant and soil types in the HAPEX case.
219 Figures 4 and 5 demonstrate that the strength of the stem-root flow is greater in LHC, with associated
220 changes in soil moisture of up to $0.1 \text{ m}^3 \text{ m}^{-3}$ compared with the maximum changes of $0.05 \text{ m}^3 \text{ m}^{-3}$ at
221 HAPEX. This is simply because LHC has more intense rainfall than HAPEX.

222

223 4. Effect of stem-root flow on energy flux

224 The results in last section show that stem-root flow can alter the vertical profile of soil moisture.
225 It is important to know whether such a modification has significant effects on evapotranspiration and

226 associated interactions between the land and atmosphere. The soil moisture in the top soil layer in the
227 LHC case generally decreased due to stem-root flow, except in some instances (e.g., mid-September,
228 the later dry season) when the enhanced moisture storage in the deep layers replenish the moisture in
229 the drying surface soil through moisture diffusion. The changes in plant transpiration, however, were
230 insignificant (red curve in Fig. 6a), as this process is associated with soil moisture not only in the top
231 layer but also in the deeper layers that are within the reach of the root system. Therefore, the effect of
232 surface layer drying on transpiration may be compensated by the moistening of the lower layers. Soil
233 moisture in these layers are well above the wilting point to support the normal transpiration.
234 Meanwhile, the drying of the surface soil resulted in less soil evaporation (Fig. 6a), which heavily
235 relies on soil moisture near soil surface, and thus weaker the total latent heat release (see Table 4 for the
236 mean and maximum changes in daily temperatures and energy fluxes). This led to a higher soil
237 surface temperature and consequently stronger sensible heat flux (blue curve in Fig. 6b), which
238 resulted in warmer air (magenta curve in Fig. 7b) and thus stronger rainwater evaporation from the leaf
239 surface (green curve in Fig. 6a).

240 In the HAPEX case, the stem-root flow caused a general drying of the top soil, except for a brief
241 period in mid-October (Fig 7a). However, responses in soil evaporation were not as straightforward
242 as in the LHC case. For example, in late July (just after the start of the growing season) there was a
243 spike in the evaporation but a reduction in the moisture of the top soil layer (blue curve in Fig 7a). As
244 wind speed is the same for both cases, the increase in soil evaporation must be due to either a higher

245 soil temperature and/or a lower water vapor density in the air near the soil surface. This was indeed
246 the case (magenta and black curves in Fig. 7b) and found to be driven by changes in transpiration.

247 Soil moisture in the HAPEX case was generally much lower than in the LHC case and
248 occasionally fell below the wilting point. The stomatal resistance that controls transpiration is very
249 sensitive to the soil moisture near the wilting point. As such, a slight decrease in the moisture of the
250 top soil layer can dramatically reduce transpiration. When soil moisture approached the wilting point
251 in late July, plant transpiration reduced sharply in response to the stem-root flow effect (red curve in
252 Fig. 7a). Such a change in plant transpiration caused an increase in the air temperature near the soil
253 surface (magenta curve in Fig. 7b) and a decrease in air humidity, which increased soil evaporation
254 (blue curve in Fig 7a). In early August, however, soil moisture accumulated in the bottom layer
255 through the stem-root flow (cf. Fig. 5c) and the stomatal resistance began to decrease such that
256 transpiration recovered and soon dominated the overall evapotranspiration throughout the rest of the
257 growing season. The increased transpiration also caused a reduction in air temperature and surface
258 temperature and thus the associated sensible heat flux (blue curve in Fig. 7b). During late August to
259 mid-September, surface soil moisture was so low in some instances (cf. Fig 5a), transpiration was
260 shutdown with or without the stem-root flow effect. In these instances, the net energy flux was
261 controlled by soil evaporation (Fig 7b).

262

263 5. Discussion

264 The above analyses indicate that stem-root flow affects the energy flux mainly through changing
265 the balance between surface soil evaporation and sensible heat fluxes in the humid environment of
266 LHC, and through changing plant transpiration and sensible heat fluxes over the relatively dry
267 environment at HAPEX. The associated changes in annual energy flux to the atmosphere are strongly
268 positive at LHC, but nearly balanced at HAPEX. However, the magnitude of the changes of the
269 individual energy flux component was significantly higher for HAPEX (peaked at approximately -67
270 and +51 W m⁻² for transpiration and sensible heat, respectively) than for LHC (peaked at
271 approximately -16 and +31 W m⁻² for evaporation and sensible heat, respectively) due to its drier
272 Mediterranean environment.

273 Another interesting contrast between the two cases is the relationship between sensible heat and
274 total heat (sensible heat plus latent heat). In the LHC case, the responses of sensible heat and total
275 heat to the stem-root flow are generally of the same sign (Fig. 6b), whereas they have opposite signs in
276 the HAPEX case (Fig. 7b). Furthermore, the net change in heat flux is dominated by sensible heat at
277 LHC but by latent heat at HAPEX. Budyko (1974) proposed two main evapotranspiration regimes:
278 soil moisture-limited and energy-limited. As summarized by Seneviratne et al. (2010), when soil
279 moisture remains above a critical value, the fraction of evapotranspiration of the total energy flux is
280 independent of the soil moisture content (energy-limited regime); below the critical soil moisture value,
281 the soil moisture content provides a first-order constraint on evapotranspiration (soil moisture-limited

282 regime). Therefore, the evapotranspiration responses to the stem-root flow as discussed above imply
283 that HAPEX is in the soil moisture-limited regime, whereas LHC is in the energy-limited regime.
284 Note that this regime separation needs to take into account the contribution of deep soil moisture to
285 transpiration.

286 Regarding the partition of water transport, recent studies (e.g., Jasechko et al., 2013; Good et al.,
287 2015; Wei et al., 2015) explored the dominant role of transpiration in ecosystem evapotranspiration.
288 The results of this work partially concur with these studies. In other words, the stem-root flow in the
289 plant-soil system could enhance the transpiration, and reduce the soil evaporation, which regulated the
290 partition of evapotranspiration. A number of PILPS studies, including the PILPS-HAPEX
291 experiment (Boone and Wetzel, 1996; Henderson-Sellers, 1995; Shao et al., 1996; Xue et al., 1996)
292 consistently demonstrated that the current land model parameterizations have the weakness in
293 simulating the soil moisture in the dry season. This study by introducing a parameterization on the
294 stem-root flow mechanisms, wish to help solve this deficiency. With the stem-root flow mechanism,
295 the soil moisture will redistribute in vertical, leading to better simulated results in each layer, which
296 is important for the evapotranspiration partition.

297 By including the stem-root flow mechanism, the land surface model appears to better simulate the
298 vertical distribution of soil moisture. However, significant discrepancies still exist in the model based
299 on comparisons with observed data. The discrepancies may be associated with uncertainties in
300 soil-related physical parameters, such as a few that we listed in the earlier sections. For example, a

301 wide range of values have been reported in the literature for the parameter V_s . In the above
302 simulations, we assigned $V_s = 10^{-4} \text{ m s}^{-1}$, which is probably at the low end of the documented values.
303 An additional simulation was performed using a 10-fold higher V_s value (i.e., $V_s = 10^{-3} \text{ m s}^{-1}$), and the
304 resulting soil moisture changes were similar to those presented in Figs. 4 and 5 with differences of only
305 a few percent and thus are barely legible in Figs. 8 and 9. When a smaller value of $V_s = 10^{-5} \text{ m s}^{-1}$
306 was used, the effect of stem-root flow on soil moisture was similar but the magnitude of the changes
307 was reduced by approximately 50%. These sensitivity tests give an indication of the uncertainties
308 associated with V_s .

309 Even with the maximum V_s , the simulated soil moistures at the bottom layer are still lower than
310 observed. More realistic values for other soil physical parameters and/or optimizations of these
311 parameters are required. Xue et al. (1996) pointed out that land surface models such as SSiB are quite
312 sensitive to soil-type dependent parameters such as the hydraulic conductivity at saturation and the
313 coefficient used to calculate soil water potential. Such parameters can vary significantly from place
314 to place, and sufficient information to assign appropriate values is usually lacking. This is
315 particularly true for LHC where the soil types exhibited a rather inhomogeneous vertical distribution,
316 and some humus layers could exist to retard surface drainage. Another critical issue is the treatment
317 of water flow across the bottom soil layer. In our current model, soil moisture can leave the bottom
318 layer with a fixed efficiency, but no recharge from the water table below is allowed. These issues
319 might cause the model to underestimate the soil moisture in the bottom layer (regardless of the

320 presence of stem-root flow), which occurred in both the LHC and HAPEX simulations (cf. Figs. 4c
321 and 5c). On the other hand, the overestimation of soil moisture in SM1 and the underestimation in
322 SM3 in spring at LHC (Fig 4) could also be explained by missing mechanisms such as hydraulic
323 redistribution (cf. Brooks et al., 2002), which provides a bypass of soil moisture through the inside of
324 the root rather than the exterior surface of the root as in the case of stem-root flow transport. On the
325 other hand, the overestimation of the middle-layer soil moisture at HAPEX may be partly
326 contributed from the plant uptake process which was not considered in this study. Besides, due to a
327 lack of observational data, we used a uniform vertical distribution of root, which might be the other
328 issue on different effects on two sites from stem-root flow. In recent years, U.S. Department of
329 Energy has supported a number of projects to measure the root vertical distribution. With more
330 data becoming available, we should be able to more realistically assess its effects. Henderson-Sellers
331 (1996) indicated that a full evaluation of land surface model's simulation against observations can be
332 established only when the initial conditions and all soil parameters are known precisely. Because
333 this study lacks of process-level data, so the improvement should be more prudent to represent.
334 Since this exploratory study focuses on introducing the stem-root flow mechanisms in a land surface
335 model and test its possible impact, we will not further test the uncertainty due to other parameters in
336 this paper. We hope more relevant measurements (such as the root distribution, stemflow to leaf
337 drainage ratio, and root flow velocity) will provide useful information to study these issues further.

338

339 6. Conclusion

340 In this study, a stem-root flow mechanism, which provides an efficient water channel for rain to
341 penetrate into deep soil, was formulated and implemented into an offline version of the SSiB
342 land-atmosphere model. The model was used to simulate soil moisture variation at two sites with
343 different climate and ecology conditions: LHC with a mountain rainforest climate and HAPEX with a
344 Mediterranean climate. The results showed that the inclusion of the stem-root flow mechanism
345 substantially improved the capability of the model to simulate vertical soil moisture profiles.
346 Stem-root flow generally caused a drying of the top soil layer (upper 20 cm) and a moistening of the
347 bottom layer (below 50 cm) in the model. On a few occasions, such as after a long dry period, the
348 surface layer may be less dry than without the stem-root flow due to greater water supply from the
349 lower layers. The middle soil layer at LHC was also moistened and, in many instances during rainfall
350 events, the moisture in this layer fluctuated more intensely than in the top layer in response to the
351 stem-root flow. However, in the HAPEX case, the middle layer became dryer with less fluctuation.
352 Due to differences in plant and soil types, the strength of the stem-root flow was greater at LHC than at
353 HAPEX.

354 The change in soil moisture associated with the stem-root flow leads to significant modifications
355 in heat and moisture fluxes between the land and atmosphere. The general drying of the surface soil
356 leads to reduced soil evaporation and thus increased soil temperature. Plant transpiration at LHC was
357 not significantly affected by the stem flow because the soil moisture content was maintained well

358 above the wilting point. Therefore, the stem-root flow related to energy flux between the soil and
359 atmosphere is mainly controlled by sensible heat. In this sense, LHC may be considered as having an
360 energy-limited evapotranspiration regime. In contrast, the HAPEX soil (especially the top layer) was
361 generally dryer and sometimes fell below the wilting point. Plant transpiration can thus be
362 substantially affected by the stem-root flow. Changes in transpiration lead to changes in air
363 temperature, which, in turn, influence soil temperature. This effect is stronger than that resulting from
364 the soil evaporation associated with changes in the soil moisture of the top soil layer. At the HAPEX
365 site, evapotranspiration was more soil moisture-limited than energy-limited, and its net change in heat
366 flux associated with the stem-root flow was dominated by latent heat. While the stem-root flow effect
367 on soil moisture was weaker there than at LHC, the energy flux exchanges were actually stronger due
368 to the sensitive transpiration process.

369 Through the impact on soil moisture profiles, stem-root flow can significantly affect evaporation
370 and transpiration processes. The associated changes in moisture and energy fluxes between the land
371 and atmosphere may affect boundary-layer stability and convective processes. As evapotranspiration
372 returns as much as 60% of the precipitation back to the atmosphere over land (Oki and Kanae, 2006),
373 the stem-root flow mechanism may be a key factor in controlling the surface water budget and
374 hydrological cycle. The enhanced storage of water in deep soil layers may have a long-term effect on
375 the climate system. These issues are worthy of further investigation through more relevant
376 observations and testing by coupling the stem-root flow mechanism with global climate models.

377

378 **Acknowledgment:** This study was supported by the Ministry of Science and Technology of the
379 Republic of China on Taiwan through project NSC-100-2119-M-002-023-MY5. Dr. Y. Xue's
380 support is from U.S. NSF AGS-1346813. We are also grateful to Dr. S. Sun for technical assistance
381 on SSiB, Drs. M.-H. Li and Y.-Y. Chen for providing observation data, and Dr. W.-L. Liang for helpful
382 suggestions. We also deeply appreciate three reviewers' efforts to provide insightful and constructive
383 comments and suggestions to improve and revise the paper.

384

385 **Appendix.** Derivation of D_{eff}

386 The parameter D_{eff} in Eq. (4) was derived in a similar fashion as in Zimmerman and Bodvarsson
387 (1991). As shown in Figure A1, the part of soil next to the root flow absorbs water and form a thin,
388 saturated boundary of width λ . A gradient of soil moisture is formed in the transition zone (of
389 width δ), with soil water potential decrease from the saturated state, Ψ_s , to that of the bulk soil, Ψ_w .
390 Diffusion of soil moisture toward the bulk soil is directly proportional to this gradient.

391 The soil moisture horizontal (x -direction) movement can be express as following:

392
$$\rho \frac{\partial \theta}{\partial t} = \frac{\partial}{\partial x} \left[K(\Psi) \frac{\partial \Psi}{\partial x} \right] \quad (\text{A1})$$

393 where ρ is soil porosity; θ is the ratio of soil moisture content to its saturated state; K (in m s^{-1}) is the
394 hydraulic conductivity of the soil; and Ψ (in m) is the soil water potential. Equation (A1) is subject
395 to the following initial and boundary conditions:

$$\theta(0, t) = 1, \theta(x, 0) = \theta_w, \theta(x \rightarrow \infty, t) = \theta_w. \quad (\text{A2})$$

The first condition means that, when the root-flow occurs, soil at the root-soil interface ($x = 0$) is saturated. The next two conditions specify the initial bulk soil moisture content, θ_w , and this value remains unaffected by the root flow at a far distance from the root-soil interface throughout the integration time period.

The hydraulic conductivity and water potential of the soil can be represented with the empirical relationship of Clapp and Hornberger (1978):

$$K(\Psi) = K_s(\Psi / \Psi_s)^{-\frac{3}{b}+2} \quad (\text{A3})$$

$$\Psi = -\Psi_s \theta^b, \quad (\text{A4})$$

where K_s (in m s^{-1}) is hydraulic conductivity at saturation; b is an empirical constant dependent on the soil type. By introducing a similarity variable η and two normalized variables $\hat{\Psi}$ and \hat{K} :

$$\eta \equiv \sqrt{\frac{\rho}{K_s \Psi_s t}}, \hat{\Psi} \equiv \frac{\Psi}{\Psi_s}, \text{ and } \hat{K} \equiv \frac{K}{K_s}, \quad (\text{A5})$$

Eq. (A1) can be transformed into

$$\frac{d}{d\eta} \left(\hat{K}(\hat{\Psi}) \frac{d\hat{\Psi}}{d\eta} \right) + \frac{\eta}{2} \frac{d\theta}{d\eta} = 0, \quad (\text{A6})$$

whereas the initial and boundary conditions in Eq. (A2) reduced to

$$\theta(0) = 1, \theta(\eta \rightarrow \infty) = \theta_w \quad (\text{A7})$$

Zimmerman and Bodvarsson (1991) showed that the solution for Eq. (A6) with conditions in Eq. (A7) can be approximated as:

$$\left\{ \begin{array}{ll} \theta = 1, & \text{if } 0 \leq \eta \leq \lambda \\ \theta = 1 - (1 - \theta_w) \frac{\eta - \lambda}{\delta}, & \text{if } \lambda < \eta \leq \lambda + \delta \\ \theta = \theta_w, & \text{if } \lambda + \delta < \eta < \infty \end{array} \right. \quad (\text{A8})$$

where

$$\delta = 2 \sqrt{\frac{b}{1 + \frac{b}{b(1 - \theta_w)}}} \quad \text{and} \quad \lambda = \frac{\delta}{b(1 - \theta_w)} \quad (\text{A9})$$

That is, within the root-soil boundary ($0 \leq \eta \leq \lambda$), θ is saturated ($=1$); whereas in the transition zone ($\lambda < \eta \leq \lambda + \delta$), θ decreases linearly from 1 to θ_w . Here, δ is the “effective thickness” of diffusion in the η coordinate, and it can be revert back to the x coordinate using the similarity conversion in Eq. (A5):

$$D_{\text{eff}} = \delta \sqrt{\frac{K_s \Psi_s t}{\rho}} \quad (\text{A10})$$

By applying the actual rainfall duration for t into Eq. (A10), we calculated the mean values of $D_{\text{eff}} = 0.005$ m for the HAPEX site and $D_{\text{eff}} = 0.03$ m for the LHC site.

Reference

- André, F., Jonard, M., and Ponette, Q.: Influence of species and rain event characteristics on stemflow volume in a temperate mixed oak–beech stand, *Hydrological Processes*, 22, 4455-4466, 10.1002/hyp.7048, 2008.
- Angevine, W. M., Bazile, E., Legain, D., and Pino, D.: Land surface spinup for episodic modeling, *Atmos. Chem. Phys.*, 14, 8165-8172, 2014.
- Beven, K., and Germann, P.: Macropores and water flow in soils, *Water Resources Research*, 18, 1311-1325, 1982.
- Böhm, W.: *Methods of studying root systems*, Springer-Verlag, 1979.

434 Boone, A. and Wetzel, P. J.: Issues related to low resolution modeling of soil moisture: experience
 435 with the PLACE model, *Global and Planetary Change*, 13, 161-181, 1996.

436 Brooks, J. R, Meinzer, F. C., Coulombe, R. and Gregg, J.: Hydraulic redistribution of soil water during
 437 summer drought in two contrasting Pacific Northwest coniferous forests. *Tree Physiology*, 22,
 438 1107-1117, 2002

439 Budyko, M. I.: *Climate and Life*, Academic Press, New York, 1974.

440 Chase, T. N., Pielke, R. A., Kittel, T. G. F., Nemani, R., and Running, S. W.: Sensitivity of a general
 441 circulation model to global changes in leaf area index, *Journal of Geophysical Research:*
 442 *Atmospheres*, 101, 7393-7408, 1996.

443 Chase, T. N., Pielke Sr, R. A., Kittel, T. G. F., Nemani, R. R., and Running, S. W.: Simulated impacts
 444 of historical land cover changes on global climate in northern winter, *Climate Dynamics*, 16,
 445 93-105, 2000.

446 Chen, Y.-Y.: *Investigating the Seasonal Variability of Surface Heat and Water Vapor Fluxes with*
 447 *Eddy Covariance Techniques: a Subtropical Evergreen Forest as an Example*, Doctoral,
 448 Graduate Institute of Hydrological and Oceanic Sciences, National Central University, 149 pp.,
 449 2012.

450 Clapp, R.B. and Homberger, G.M.: Empirical equations for some soil hydraulic properties, *Water*
 451 *Resour. Res.*, 14: 601-604, 1978.

452 de Goncalves, L. G. G., Shuttleworth, W. J., Burke, E. J. , Houser, P., Toll, D. L., Rodell, M. and
 453 Arsenault, K.: Toward a South America Land Data Assimilation System: Aspects of land
 454 surface model spin-up using the Simplified Simple Biosphere, *J. Geophys. Res.*, 111,
 455 D17110,2006.

456 Dorman, J. L., and Sellers, P. J.: A Global climatology of albedo, roughness length and stomatal
 457 resistance for atmospheric general circulation models as represented by the Simple Biosphere
 458 Model (SiB), *Journal of Applied Meteorology*, 28, 833-855, 1989.

459 Gerke, H.: Bypass flow in soil, in: *Encyclopedia of Agrophysics*, edited by: Gliński, J., Horabik, J.,

460 and Lipiec, J., Encyclopedia of Earth Sciences Series, Springer Netherlands, 100-105, 2014.
 461 Good, S. P., Noone, D., and Bowen, G.: Hydrologic connectivity constrains partitioning of global
 462 terrestrial water fluxes, *Science*, 349(6244), 175–177, 2015.
 463 Goutorbe, J.-P., J. Noilhan, C. Valancogne, and Cuenca, R. H.: Soil moisture variations during
 464 HAPEX-MOBILHY, *Annals of Geophysics*, 7, 415-426, 1989.
 465 Goutorbe, J. P.: A Critical assessment of the Samer network accuracy, in: *Land Surface Evaporation*,
 466 edited by: Schmugge, T., and André, J.-C., Springer New York, 171-182, 1991.
 467 Goutorbe, J. P., and Tarrieu, C.: HAPEX-MOBILHY data base, in: *Land Surface Evaporation*, edited
 468 by: Schmugge, T., and André, J.-C., Springer New York, 403-410, 1991.
 469 Henderson-Sellers, A., Pitman, A. J., Love, P. K., Irannejad, P. and Chen, T. H.: The Project for
 470 Intercomparison of Land Surface Parameterization Schemes (PILPS): Phases 2 and 3. *Bull.*
 471 *Amer. Meteor. Soc.*, 76, 489-503, 1995
 472 Henderson-Sellers, A.: Soil moisture simulation: Achievements of the RICE and PILPS
 473 intercomparison workshop and future directions. *Global Planet. Chang.*, **13**, Issues 1–4,
 474 99-115, 1996
 475 Jarvis, N. J., and Dubus, I. G.: State-of-the-art review on preferential flow, www.eu-footprint.org, 60
 476 pp., 2006.
 477 Jasechko, S., Sharp, Z. D., Gibson, J. J., Birks, S. J., Yi, Y. and Fawcett, P. J.: Terrestrial water fluxes
 478 dominated by transpiration, *Nature*, 496(7445), 2013.
 479 Johnson, M. S., and Lehmann, J.: Double-funneling of trees: stemflow and root-induced preferential
 480 flow, *Ecoscience*, 13, 324-333, 2006.
 481 Köhne, J. M., Köhne, S., and Šimůnek, J.: A review of model applications for structured soils: a)
 482 Water flow and tracer transport, *Journal of Contaminant Hydrology*, 104, 4-35, 2009.
 483 Levias, D. F., and Frost, E. E.: A review and evaluation of stemflow literature in the hydrological and
 484 biochemical cycles of forested and agricultural ecosystems., *Journal of Hydrology*, 274, 1-29,
 485 2003.

486 Levia, D. F., and Germer, S.: A review of stemflow generation dynamics and stemflow-environment
487 interactions in forests and shrublands, *Rev. Geophys.*, 53, 673–714, 2015.

488 Li, J., He, B., Chen, Y., Huang, R., Tao, J., and Tian, T.: Root distribution features of typical herb
489 plants for slope protection and their effects on soil shear strength, *Transactions of the Chinese*
490 *Society of Agricultural Engineering*, 29, 144-152, 2013.

491 Li, X.-Y., Yang, Z.-P., Li, Y.-T., and Lin, H.: Connecting ecohydrology and hydrology in desert
492 shrubs: stemflow as a source of preferential flow in soils, *Hydrology and Earth System*
493 *Sciences*, 13, 1133-1144, 2009.

494 Li, X.-Y., Lin, H., and Levia, D. F.: Coupling ecohydrology and hydrology at different
495 spatio-temporal scales in water-limited ecosystems, in: *Hydrology*, edited by: Lin, H.,
496 Academic Press, Boston, 737-758, 2012.

497 Liang, W.-L., Kosugi, K. i., and Mizuyama, T.: Heterogeneous soil water dynamics around a tree
498 growing on a steep hillslope, *Vadose Zone J.*, 6, 879-889, 2007.

499 Liang, W.-L., Kosugi, K. i., and Mizuyama, T.: A three-dimensional model of the effect of stemflow
500 on soil water dynamics around a tree on a hillslope. *J. Hydro.*, 366(1-4), 62-75, 2009.

501 Lim, Y.- J., Hong, J., Lee, T.-Y.: Spin-up behavior of soil moisture content over East Asia in a land
502 surface model, *Meteorology and Atmospheric Physics*, 118(3), 151-161, 2012.

503 Liu, I.-W. Y., Waldron, L. J., and Wong, S. T. S.: Application of nuclear magnetic resonance imaging
504 to study preferential water flow through root channels, *Tomography of Soil-Water-Root*
505 *Processes*, 135-148, 1994.

506 McGuffie, K., Henderson-Sellers, A., Zhang, H., Durbidge, T. B., and Pitman, A. J.: Global climate
507 sensitivity to tropical deforestation, *Global and Planetary Change*, 10, 97-128, 1995.

508 Návar, J.: The causes of stemflow variation in three semi-arid growing species of northeastern
509 Mexico, *Journal of Hydrology*, 145, 175-190, 1993.

510 Neave, M., and Abrahams, A. D.: Vegetation influences on water yields from grassland and
511 shrubland ecosystems in the Chihuahuan Desert, *Earth Surface Processes and Landforms*, 27,

2002.

Oki, T. and Kanae, S.: Global Hydrological Cycles and World Water Resources. *Science*, **313**, 1068-1072, 2006.

Sellers, P. J., Mintz, Y., Sud, Y. C., and Dalcher, A.: A Simple Biosphere Model (SIB) for use within general circulation models, *Journal of the Atmospheric Sciences*, 43, 505-531, 1986.

Seneviratne, S. I., Corti, T., Davin, E. L., Hirschi, M., Jaeger, E. B., Lehner, I., Orlowsky, B., and Teuling, A. J.: Investigating soil moisture–climate interactions in a changing climate: A review, *Earth-Science Reviews*, 99, 125-161, 2010.

Shao, Y., Anne, R. D., Henderson-Sellers, A., Irannejad, P., Thorton, P., Liang, X., Chen, T. H., Ciret, C., Desborough, C., Barachova, O., Haxeltine, A. and Ducharne, A.: Soil Moisture Simulation, A report of the RICE and PILPS Workshop. GEWEX Tech. Note, IGPO Publ. Ser., 14, 179 pp, 1995.

Siegert, C. M., and Levia, D. F.: Seasonal and meteorological effects on differential stemflow funneling ratios for two deciduous tree species, *Journal of Hydrology*, 519, Part A, 446-454, 2014.

Tanaka, T., Taniguchi, M., and Tsujimura, M.: Significance of stemflow in groundwater recharge. 2: A cylindrical infiltration model for evaluating the stemflow contribution to groundwater recharge, *Hydrological Processes*, 10, 81-88, 1996.

Taniguchi, M., Tsujimura, M., and Tanaka, T.: Significance of stemflow in groundwater recharge. 1: Evaluation of the stemflow contribution to recharge using a mass balance approach, *Hydrological Processes*, 10, 71-80, 1996.

Wei, Z., Yoshimura, K., Okazaki, A., Kim, W., Liu, Z., and Yokoi, M.: Partitioning of evapotranspiration using high-frequency water vapor isotopic measurement over a rice paddy field, *Water Resources Research*, 51, 3716–3729, 2015.

Wu, B.-Y.: Simulations of Land Surface Fluxes of the Lien Hua Chih Experimental Watershed with Land Process Models, Master, Graduate Institute of Hydrological and Oceanic Sciences,

538 National Central University, 100 pp., 2011.

539 Xue, Y., Sellers, P., Kinter, J., and Shukla, J.: A simplified biosphere model for global climate studies.
540 *J. Climate*, **4**, 345-364, 1991.

541 Xue, Y., Zeng, F. J., and Adam Schlosser, C.: SSiB and its sensitivity to soil properties—a case study
542 using HAPEX-Mobilhy data, *Global and Planetary Change*, 13, 183-194, 1996.

543 Yang, Y., Uddstrom, M., and Duncan, M.: Effects of short spin-up periods on soil moisture
544 simulation and the causes over New Zealand, *J. Geophys. Res.*, 116, D24108.

545 Zhang, Y.-Q., Q. K. Zhu, and Qi, S.: Root system distribution characteristics of plants on the terrace
546 banks and their impact on soil moisture, *Acta Ecologica Sinica*, 25, 500-506, 2005.

547 Zhao, M., Pitman, A. J., and Chase, T.: The impact of land cover change on the atmospheric
548 circulation, *Climate Dynamics*, 17, 467-477, 2001.

549 Zimmerman, R. and Bodvarsson, G.: A simple approximate solution for horizontal infiltration in a
550 Brooks-Corey medium. *Transport in Porous Media*, **6**, 195-205, 1991.

553

554 Table 1. Basic parameters used for describing the LHC and HAPEX sites. LHC data were obtained
 555 from Wu (2011); HAPEX data were obtained from Goutorbe et al. (1989).

Location	LHC	HAPEX
Annual rainfall	2317 mm	856 mm
Mean temperature	19.7°C	8.6°C
Altitude	770 m	113 m
Vegetation cover	Rainforest of mixed evergreens and hardwoods	Soya crop
Soil type	Loam	17% clay content, 46% silt, 37% sand
Soil moisture measurement depth	10, 30, 50, 70, 90 cm	Every 10 cm down to 160 cm
Soil wetness exponent	2.5	5.66
Soil tension at saturation	-0.1 m	-0.30 m
Hydraulic conductivity at saturation	$1 \times 10^{-6} \text{ m s}^{-1}$	$4 \times 10^{-6} \text{ m s}^{-1}$
Soil porosity	0.530	0.446
Slope	0.55	0.05

556

557

558 Table 2. Monthly leaf area index values (in $\text{m}^2 \text{ m}^{-2}$) for LHC in 2010 and HAPEX in 1986. LHC
 559 data were obtained from Wu (2011); HAPEX data were obtained from Goutorbe et al. (1989).

Month	1	2	3	4	5	6	7	8	9	10	11	12
LHC	3.34	3.08	3.06	3.04	4.35	4.77	4.84	4.91	4.66	4.4	4.2	4.25
HAPEX	0	0	0	0	1	3	3	3	3	0	0	0

560

561

562

563 Table 3. The mean bias, root-mean-square error (RMSE), and standard deviation (STD) in simulated
564 soil moisture comparing to observations (obs). “Control” stands for simulations without the
565 stem-root flow mechanism, and “SLR90%” or “SLR50%” are simulations with the optimal stemflow
566 to leaf drainage ratio. Unit: $\text{m}^3 \text{m}^{-3}$

	SM1			SM2			SM3		
	bias	RMSE	STD	bias	RMSE	STD	bias	RMSE	STD
LHC control-obs	-0.003	0.142	0.142	-0.098	0.153	0.012	-0.141	0.193	0.131
LHC SLR90%-obs	0.023	0.056	0.051	-0.034	0.050	0.036	-0.038	0.048	0.029
HAPEX control-obs	0.018	0.036	0.032	0.032	0.037	0.019	-0.057	0.085	0.063
HAPEX SLR50%-obs	0.009	0.030	0.029	0.024	0.030	0.018	-0.049	0.074	0.056

567

568

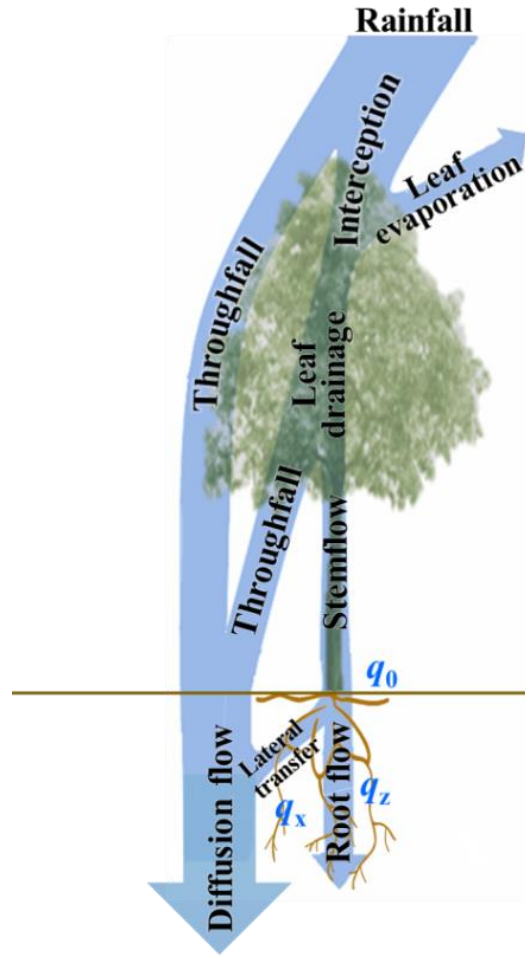
569 Table 4. Mean and maximum changes in daily temperatures and energy fluxes due to the stem-root
570 flow (between optimal SLR run and control run) during the growing season. Canopy air temperature
571 (T_C), soil surface temperature (T_S) and leaf temperature (T_L) are in $^{\circ}\text{C}$; Transpiration (TR), soil
572 evaporation (SE), leaf evaporation (LE), sensible heat (SH) and latent heat (LH) are in W m^{-2} .

	ΔT_C	ΔT_S	ΔT_L	ΔTR	ΔSE	ΔLE	ΔSH	ΔLH
LHC mean	0.32	0.31	0.34	0.20	-1.19	0.31	2.02	-0.68
LHC maximum	2.90	2.59	3.18	1.01	-15.50	11.34	31.44	-16.81
HAPEX mean	0.04	0.11	0.03	1.06	-2.17	0.28	0.52	-0.82
HAPEX maximum	1.27	1.63	1.70	-66.74	-19.5	9.95	51.16	-66.29

573

574

575

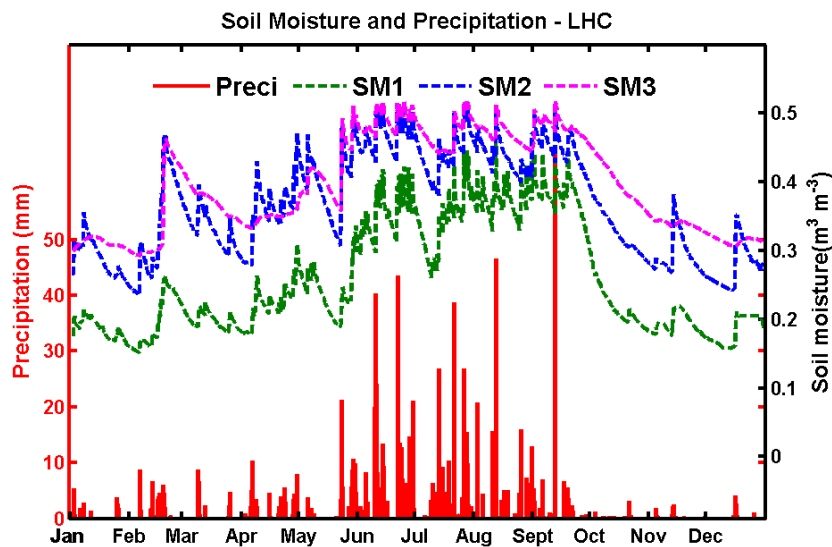


576

577 Figure 1. Stem-root flow conceptual diagram. Leaf drainage in the model can be separated into
 578 throughfall and stemflow. Following the stemflow path, rainwater can continue via the root system to
 579 reach deep soil layers and the water table. The stemflow that reaches the soil top, q_0 , is divided into a
 580 downward transfer flux (i.e., the root flow) q_z and a lateral transfer flux q_x (from the root surface to the
 581 soil), and the two transfer fluxes regulate the root flow thickness.

582

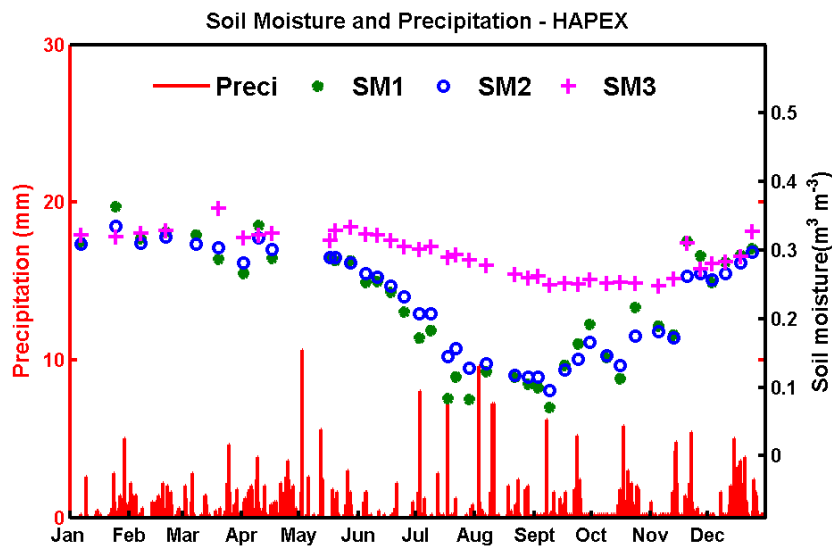
583



584

585 Figure 2. The hourly soil moisture (curves, right axis) and precipitation (red bars, left axis) observed
586 at LHC during 2010. SM1, SM2 and SM3 represent soil moisture at 10 cm (green-dashed curve), 40
587 cm (blue-dashed curve; average of 30 cm and 50 cm observations) and 90 cm (magenta-dashed curve),
588 respectively.

589



590

591 Figure 3. The weekly soil moisture (symbols, right axis) and hourly precipitation (red bars, left axis)
592 observed at HAPEX during 1986. SM1 SM2 and SM3 represent the mean soil moisture in the 0–20
593 cm (green dot), 20–50 cm (blue circle), and 50–160 cm (magenta cross) layers, respectively.

594

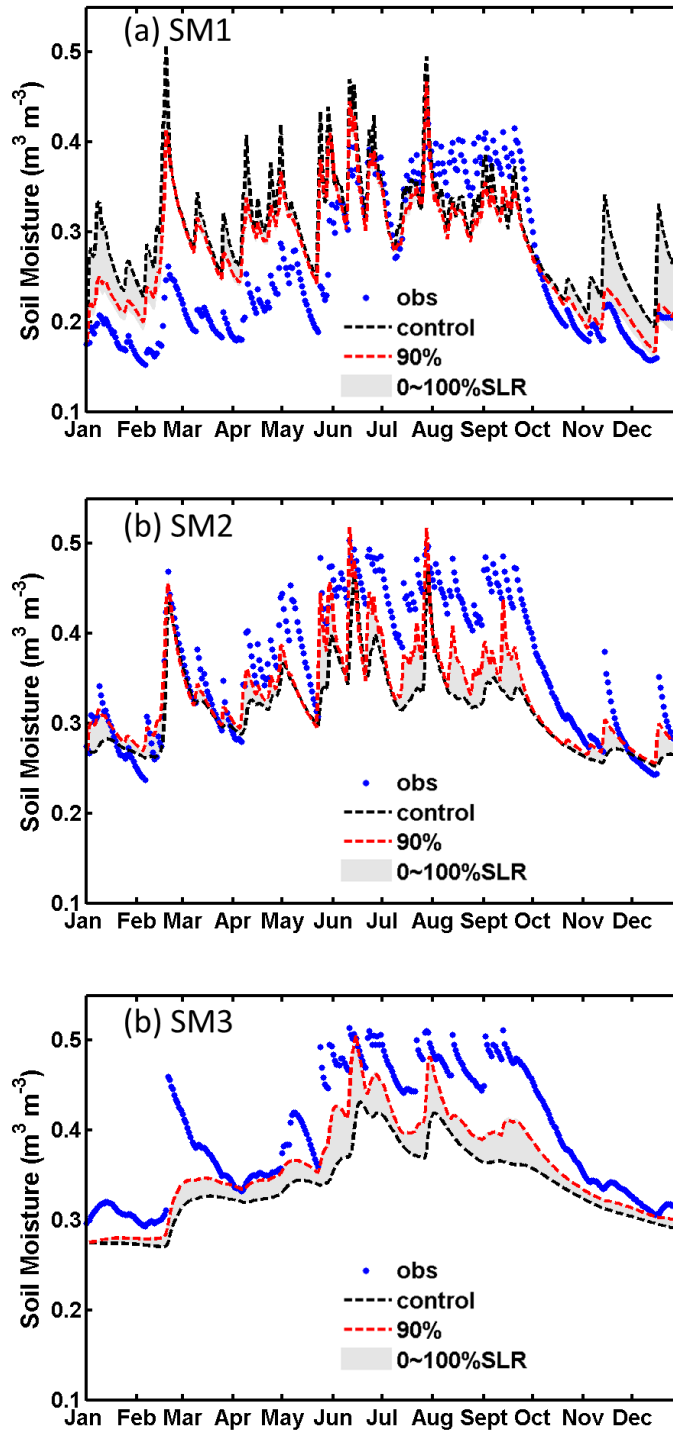


Figure 4. Simulated and observed soil moisture for the LHC site at depths of (a) SM1 (0-20 cm), (b) SM2 (20-70 cm), and (c) SM3 (70-170 cm). Observed results are shown as blue dots. Simulations with SLR=0 (i.e., control run, without stem-root flow) and SLR=90% are shown as black-dashed and red-dashed curves, respectively. The area of grey shading enclosed by SLR=0% and 100% indicates the possible range of the stem-root flow effects. All simulation results are daily averages.

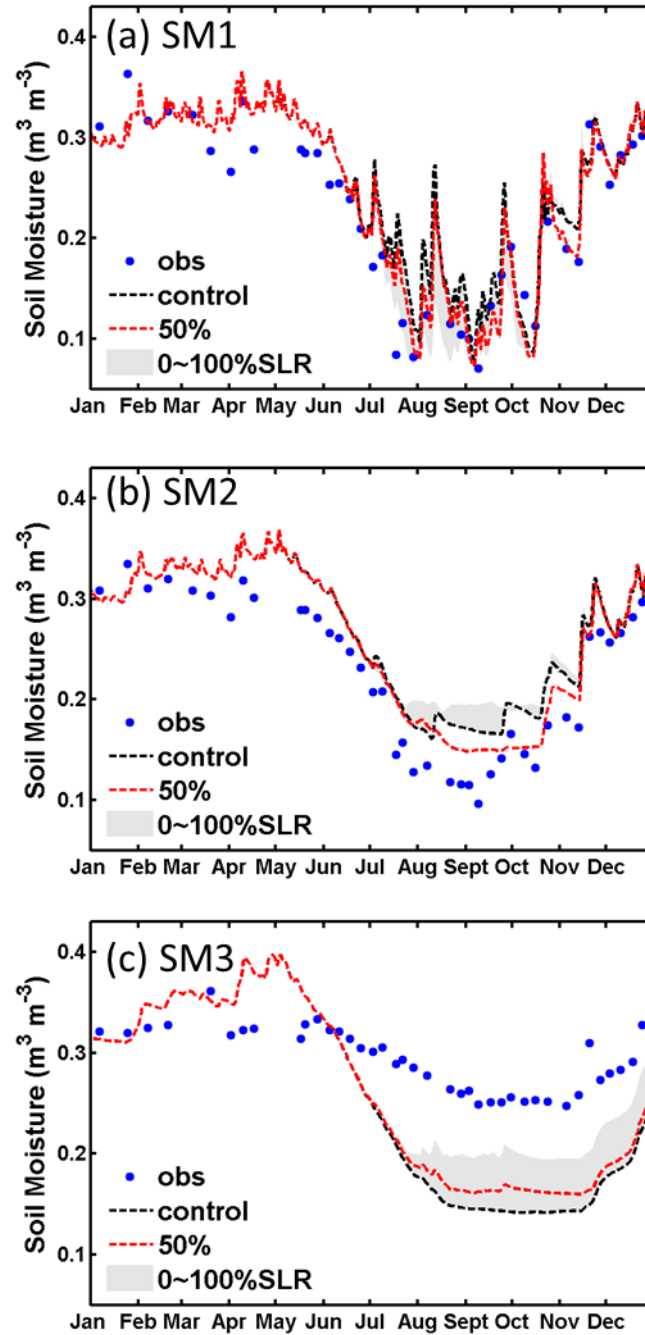


Figure 5. Same as Fig. 4, but for the HAPEX case at depths of (a) SM1 (0-20 cm), (b) SM2 (20-50 cm), and (c) SM3 (50-160 cm). Red-dashed curves are results with SLR=50%.

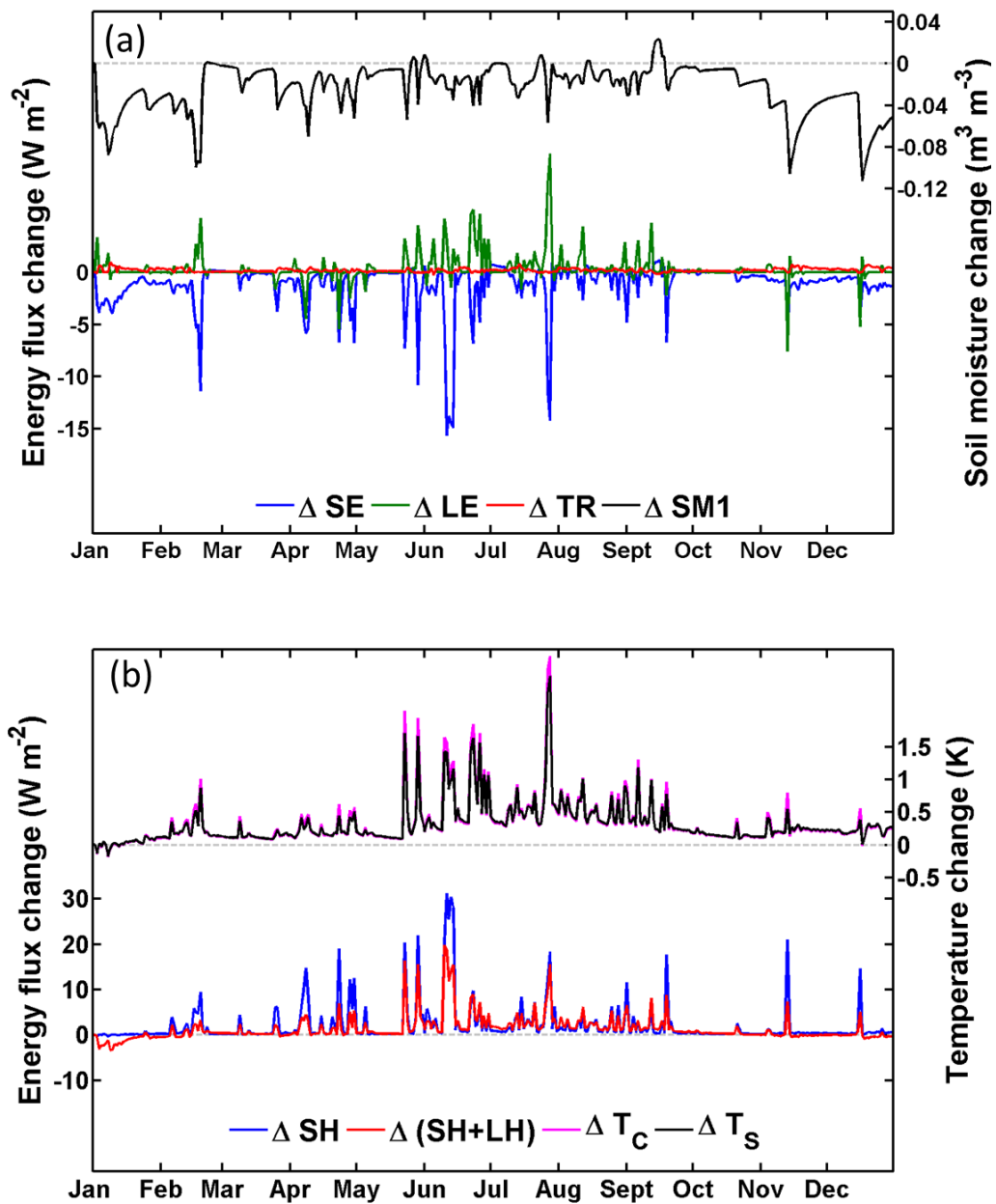
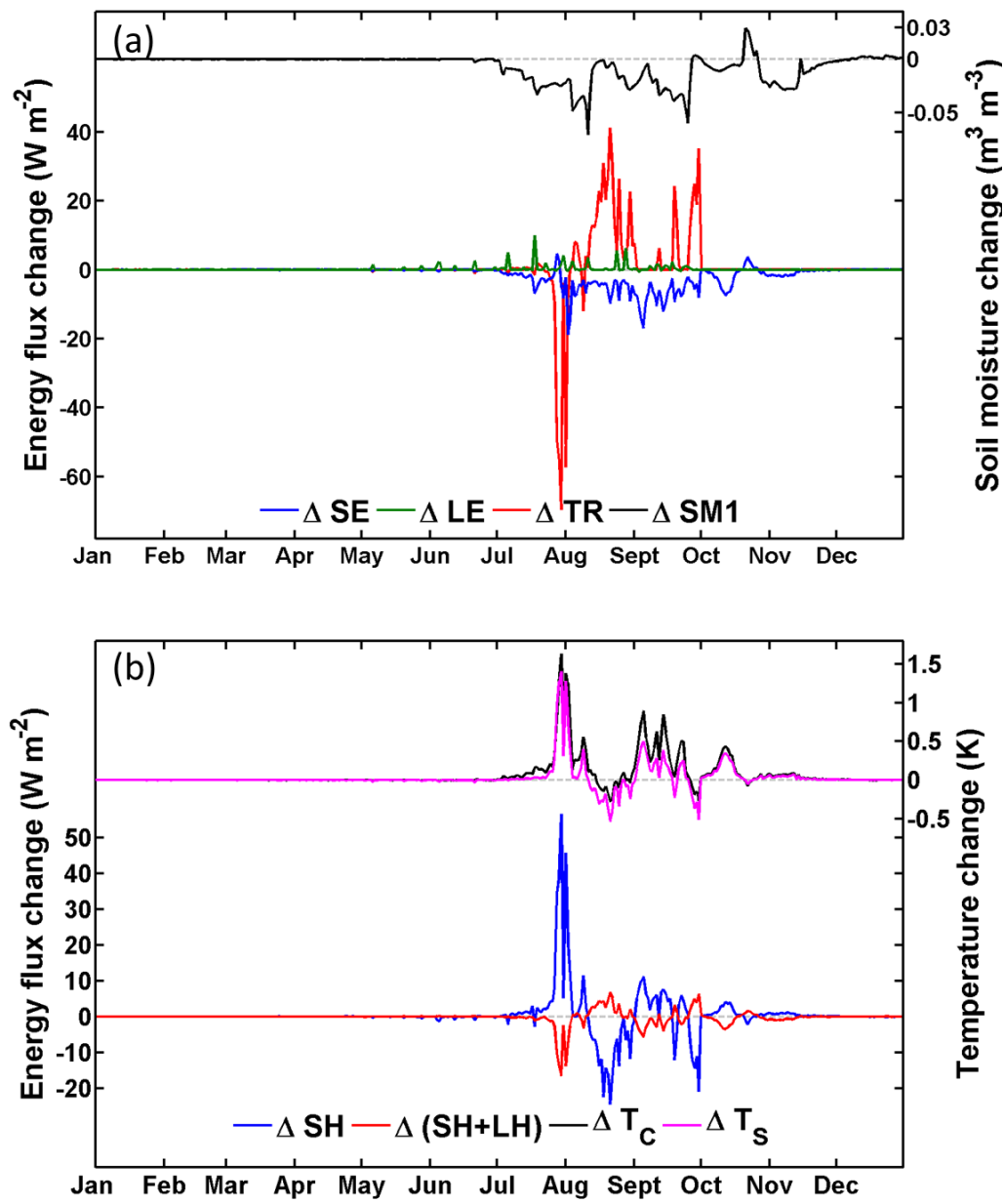


Figure 6. Difference in daily mean heat fluxes and soil moisture due to stem-root flow at the LHC case. (a) Changes in soil evaporation (SE; blue curve), leaf evaporation (LE; green curve), transpiration (TR; red curve) and soil moisture of the surface layer (SM1; black curve; right axis); (b) Changes in sensible heat (SH; blue curve), total heat (sensible heat plus latent heat (SH+LH); red curve), canopy air temperature (T_c ; magenta curve; right axis) and soil temperature (T_s ; black curve; right axis). Grey dashed lines indicate the zero baseline.



615

616 Figure 7. Same as Fig. 6, but for the HAPEX case.

617

618

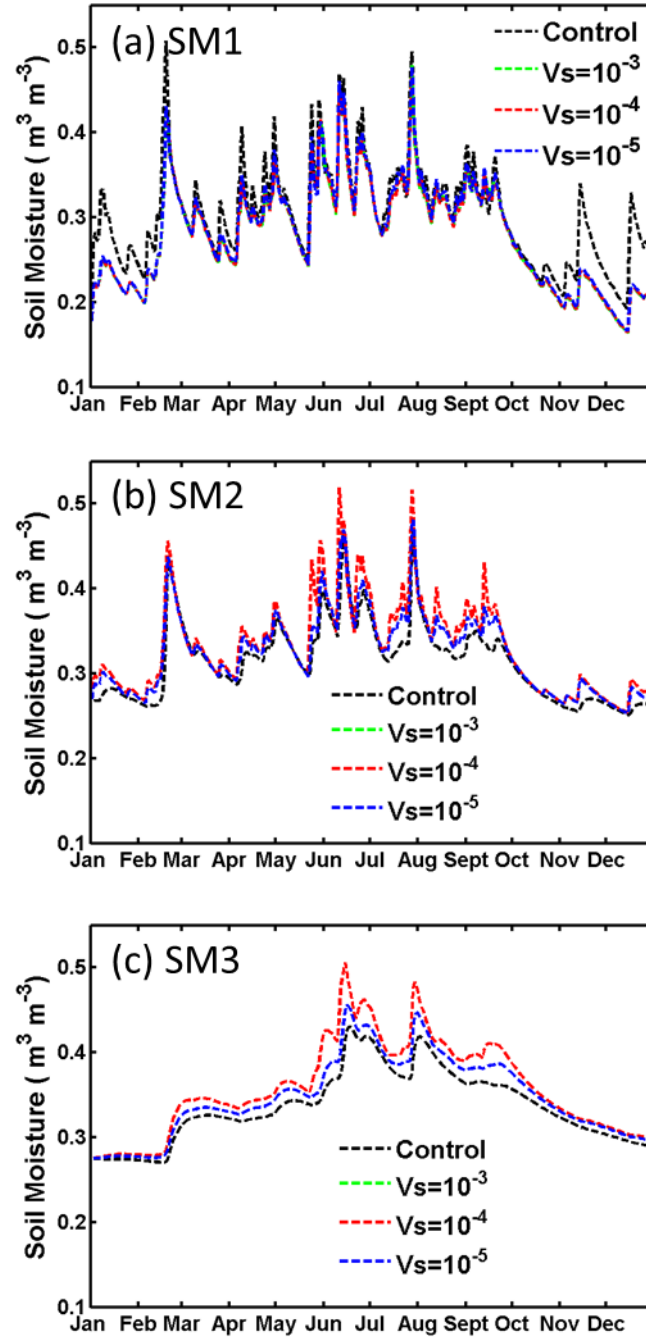
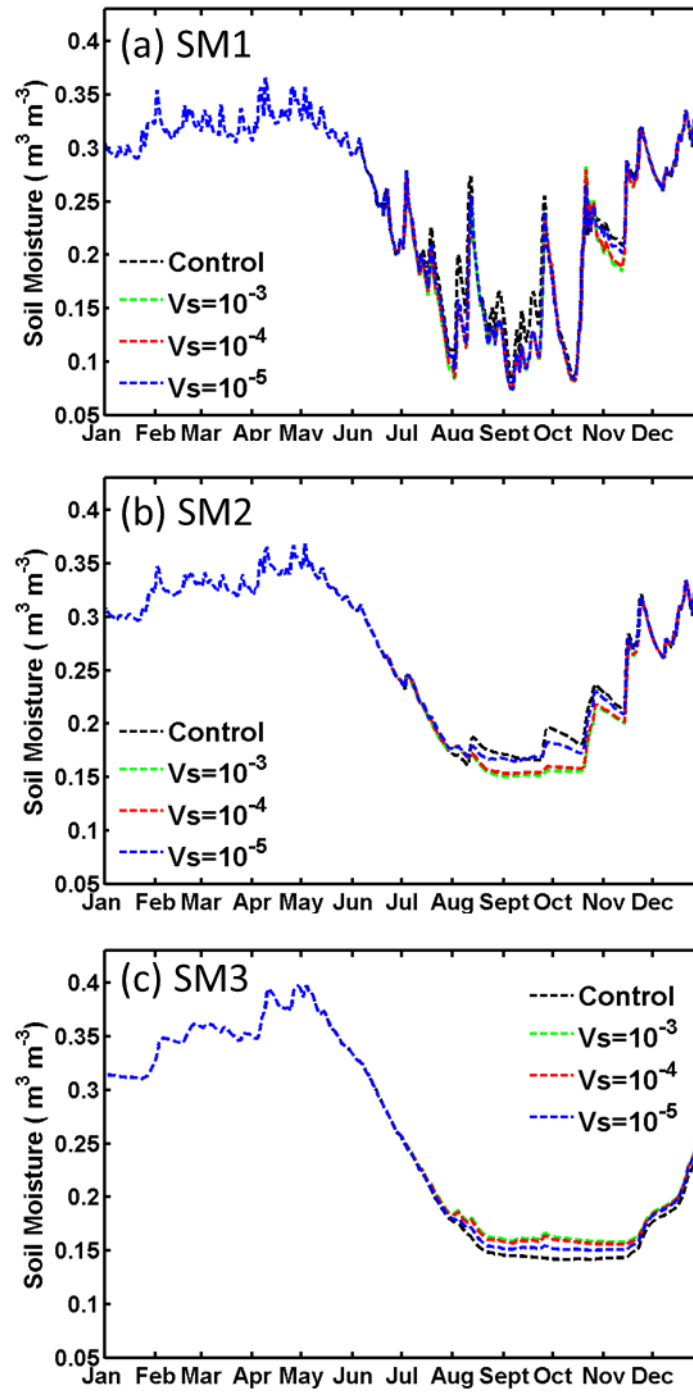


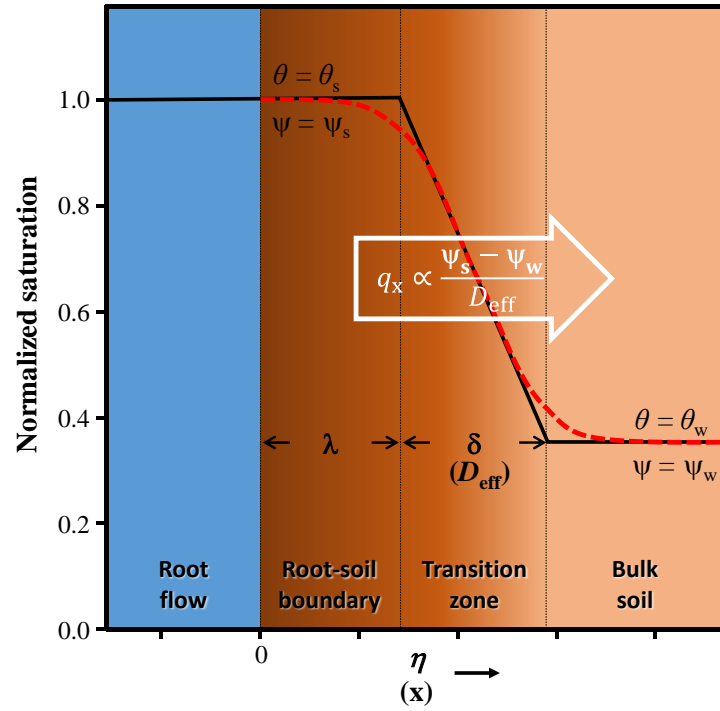
Figure 8. Sensitivity test on V_s for the LHC case with optimal SLR=90% at depths of (a) SM1 (0-20 cm), (b) SM2 (20-70 cm), and (c) SM3 (70-170 cm). The green-dashed, red-dashed and blue-dashed curves are for $V_s = 10^{-3}$, 10^{-4} , and 10^{-5} m s^{-1} , respectively. Also shown in black-dashed curves are the control run results (i.e., SLR=0).



625

626 Figure 9. Same as Fig. 8, but SLR=50% for the HAPEX case at depths of (a) SM1 (0-20 cm), (b)
 627 SM2 (20-50 cm), and (c) SM3 (50-160 cm).

628



629

630 Figure A1. Schematics of the root flow-soil boundary and soil moisture transition for the

631 parameterization of horizontal water flux q_x . The red-dashed line represents the analytical solution,

632 and the black-solid line represents the parameterization. Soil moisture is saturated ($=\theta_s$) in the

633 root-soil boundary (width λ), and decreases linearly in the transition zone (width δ) before reaching

634 that of the bulk soil (θ_w).